Colour centre recovery in yttria-stabilised zirconia: photo-induced versus thermal processes

Jean-Marc Costantini, Nadia Touati, Laurent Binet, Gerald Lelong, Maxime Guillaumet, François Beuneu

COLOUR CENTRE RECOVERY IN YTTRIA-STABILIZED ZIRCONIA: PHOTO-INDUCED VERSUS THERMAL PROCESSES

Jean-Marc COSTANTINI[1],

DEN, Service de Recherches Métallurgiques Appliquées, CEA, Université Paris-Saclay, F-91191, Gif-sur Yvette Cedex, France.

Nadia TOUATI, Laurent BINET

Chimie Paris-Tech, Rue Pierre et Marie Curie, F-75506, Paris, France

Gérald LELONG, Maxime GUILLAUMET,

Institut de Minéralogie, de Physique des Matériaux et Cosmochimie (IMPMC), Sorbonne Universités – UPMC Univ Paris 06, UMR CNRS 7590, Muséum National d'Histoire Naturelle, IRD UMR 206, 4 Place Jussieu, F-75005 Paris, France

and François BEUNEU,

LSI, CEA-CNRS-Ecole Polytechnique, F-91128 Palaiseau Cedex, France

ABSTRACT

The photo-annealing of colour centres in yttria-stabilized zirconia (YSZ) was studied by electron paramagnetic resonance spectroscopy upon UV-ray or laser light illumination, and compared to thermal annealing. Stable hole centres (HCs) were produced in as-grown YSZ single crystals by UV-ray irradiation at room temperature. The numbers of HCs decays to

[1] Corresponding author's email : jean-marc.costantini@cea.fr

non-zero asymptotic values when UV light is set off. The HCs produced by 200-MeV Au ion irradiation are partially bleached by UV light, whereas the F^+-type centres (involving oxygen vacancies) were left unchanged. In contrast, a significant photo-annealing of the latter point defects was achieved in 1.4-MeV electron-irradiated YSZ by 553-nm laser light irradiation, inside the absorption band of F^+-type centres centred at a wavelength ~550 nm. Thermal annealing of F^+-type centres was also followed by UV-visible absorption spectroscopy. Almost complete photo-bleaching by laser irradiation was achieved like for thermal bleaching at ~500K. Kinetic rate models of colour-centre evolution are proposed for the photo-induced processes and correlated to the thermally-activated ones.

Keywords: Colour centres; electron irradiation; ion irradiation; electron paramagnetic resonance spectroscopy; UV-visible optical absorption spectroscopy; photo-induced processes; yttria-stabilized zirconia.

PACS codes: 61.80.-x ; 61.72.jn ; 77.84.Bw ; 76.30.Mi ; 78.40.Fy, 78.40.Ha

I. INTRODUCTION

Colour-centre production and annealing induced by UV-light illumination was already studied in X-ray irradiated cubic yttria-stabilized zirconia (YSZ) and calcia-stabilized zirconia (CaSZ) [Azzoni, 1996]. It was shown that a complex equilibrium process occurs upon UV-light illumination at room temperature (RT) between the so-called T centres (i.e. Zr^{3+} ions sitting in a trigonal symmetry site), and oxygen hole-centres (O^- centres with an orthorhombic site symmetry) that were produced by X-ray irradiation in these single crystals [Merino, 1989; Orera, 1990; Azzoni, 1989, 1991, 1995], prior to UV-ray irradiation. Such photo-induced processes that are often overlooked may turn out to be very important for point-defect evolution under radiation. In particular, they can occur for complex radiation fields encountered in nuclear applications where broad photon spectra are generated.

More recently, we provided experimental evidence of the production of T centres and new paramagnetic centres in YSZ single crystals (with 9.5 and 18 mol% Y_2O_3) by electron or heavy-ion irradiations [Costantini, 2004, 2011]. The electron paramagnetic resonance (EPR) lines were assigned to three different colour centres: i) T-centres (similar to the X-ray induced T centres [Orera, 1990]) with a large g-factor anisotropy ($g_\perp = 1.855$, $g_{//} = 1.986$) and two native nearest-neighbour (NN) oxygen vacancies ($V_O^{\cdot\cdot}$) oriented along <111> (i.e. $[V_O^{\cdot\cdot} Zr'_{Zr} V_O^{\cdot\cdot}]^{\cdots}$ in the Kröger-Vink notation, used hereafter); ii) F^+-type centres (involving singly-ionized oxygen vacancies, $V_O^{\cdot}$, most likely oxygen divacancies, F_2^+ centres, e.g. $[V_O^{\cdot} V_O^{x}]^{\cdot}$) with a smaller g-factor anisotropy ($g_\perp = 1.972$, $g_{//} = 1.996$) and oriented along <100>; and iii) isotropic hole-centres (HCs), enhanced by the yttria content, that are different from the X-ray induced O^- centres ($[O_O^{\cdot} Y_{Zr}']^x$), with strong anisotropy [Orera, 1990].

We have shown that F^+-type centres and T centres are intrinsic electron centres: F^+-type centres are produced by elastic-collision (or nuclear-collision) processes, whereas T

centres are produced by the inelastic ones (electronic excitations and ionizations) [Costantini, 2013]. Broad optical absorption bands centred at photon energies ~2.4 eV and ~3.3 eV were found for the F^+-type centres and T centres, respectively [Costantini, 2010]. The linear correlations between the maximum absorption coefficients of those bands and colour centre concentrations (deduced from EPR spectra) yielded oscillator strengths of ~0.2 and 0.3, respectively. Upon thermal annealing, an equilibrium process was found to take place between those two colour centres leading to a non-zero asymptotic concentration of F^+-type centres for long isothermal annealing times [Costantini, 2006; 2014a].

The present study aims at investigating the photo-induced processes of colour centres at RT in electron or ion-irradiated YSZ. We show that recovery processes definitely occur for HCs and F^+-type centres upon UV-ray irradiation or selective laser light excitation, respectively. Kinetic rate models are proposed to account for both photo-annealing effects. Moreover, new results on the thermal annealing of F^+-type centres are reported on the basis of UV-visible optical absorption data, in very good agreement with previous EPR data.

II. EXPERIMENTAL PROCEDURES

II.1 SAMPLES

Yttria-stabilized zirconia (YSZ) (100) (ZrO_2: Y) single crystal plates (with 9.5 mol% Y_2O_3) provided by the Crystal-GmbH Company (Berlin, Germany) were used with thickness of 500 µm. The as-grown single crystals were colourless and transparent with an optical band gap (E_g) ~4.2 eV [Camagni, 1992]. It is known that they contain about 10 at% (non-magnetic) doubly ionized oxygen vacancies ($V_O^{\cdot\cdot}$) (devoid of electrons) with a 2+ charge state induced by charge compensation of Y^{3+} substituted for Zr^{4+} ions [Zacate, 2000].

II.2 ELECTRON AND ^{197}Au IRRADIATIONS

Electron irradiations were performed at the SIRIUS accelerator (LSI, Ecole Polytechnique, Palaiseau, France) under helium gas at around 35°C with energy of 1.4 MeV, flux of ~10^{13} cm^{-2} s^{-1} and fluence of 2.1x10^{18} cm^{-2}. The electrons were transmitted through the samples and homogeneous irradiation was achieved in the bulk. Irradiation with 200 MeV ^{197}Au ions at RT was achieved at the VIVITRON (Strasbourg, France) with a low flux of ~10^{9} cm^{-2} s^{-1} and fluences of 1x10^{12} and 2.5x10^{13} cm^{-2}. Another irradiation with 2.24 GeV ^{197}Au ions at RT was carried out at GSI-UNILAC (Helmholtz Centre for Heavy Ion Research, Darmstadt, Germany) with a flux of ~10^{9} cm^{-2} s^{-1} and fluence of 1x10^{12} cm^{-2}.

Irradiation features were computed with the ESTAR code [ICRU, 1984] for the electrons and the SRIM-2007 code [Biersack, 1980] for the ions (Table I). Absorbed doses by inelastic processes and concentrations of displaced atoms by elastic collisions were estimated for these irradiations (Table I). Similar values are obtained, on the one hand, for both Au ion irradiations at the same fluence of 1x10^{12} cm^{-2}, and on the other hand, for the electron and 2.24-GeV Au ion irradiations.

II.3 ELECTRON PARAMAGNETIC RESONANCE

Electron paramagnetic resonance (EPR) measurements were carried out at RT with the static magnetic field B//<100> using a Bruker EMX X-band spectrometer operating at 9.6 GHz. Photo-excitation experiments were performed by illuminating as-grown and 200-MeV Au-ion irradiated samples in the EPR cavity either with a Müller® Xe arc-lamp, equipped with a focusing quartz lens system, or an Omnicure® Hg vapor arc-lamp (series 2000) by using an optical fibre. The former lamp provided a broad-band white spectrum with wavelengths (λ) ranging from 250 to 1150 nm, with some sharp emission features above 800 nm, i.e. for a

range of photon energies (ħω) between ~1.1 and 5 eV. The latter one provided a spectrum ranging from 295 to 500 nm, with rather sharp emission lines between 350 and 450 nm, i.e. for photon energies ranging between ~2.5 and 4.2 eV. The recording time of EPR spectra was set to 80 seconds.

Other experiments on the electron-irradiated sample were using an Oxxius® laser diode (LD) system providing a selective photo-excitation at λ = 553 nm (i.e. ħω ~2.24 eV) by using an optical fibre. Three different laser power values were used (52, 80, and 105 mW). A similar time-sequence of illumination was applied for all samples, with time steps of 1 minute and 30 seconds between EPR spectra measurements for the UV-ray and laser irradiations, respectively. A fast field scan (10 s) was selected for recording the EPR spectra with a micro-wave power of 20 mW. A control experiment was also conducted on a virgin sample in the same conditions for a laser power of 105 mW. For the Au-ion irradiated samples, EPR lines were simulated with Lorentzian curves and integrated intensities were deduced from a least-square fitting procedure. The number of paramagnetic centres was then deduced from a calibration using a copper sulphate reference sample. For the electron-irradiated sample, only intensities of EPR lines were used. A carbon sample was measured as a g-factor reference (g = 2.025). The estimated uncertainty on the g-factor values is $\pm$ 0.001.

II.4 OPTICAL ABSORPTION SPECTROSCOPY

In-situ high-temperature annealing measurements were carried out on the 2.24-GeV Au-ion irradiated sample by using a TS1500® micro-thermometric stage adapted to the Perkin-Elmer Lambda-1050® spectrometer equipped with a Cassegrain-type microscope. The

measurements were carried out using a focal spot of 120 µm and a wavelength step of 2 nm [Chassé, 2015].Isochronal annealing for 3 minutes was performed at different temperatures from RT up to 250°C (1°C) by steps of 50°C. A heating rate of 100-150°C min^{-1} between steps was used. Isochronal annealing was monitored by recording transmitted UV-Visible-NIR absorption spectra after stabilizing temperature. The spectrum of the virgin sample, corresponding to the non-irradiated sample measured at the same temperature, was then subtracted from the raw spectra for each temperature. More experimental details are given in a previous paper [Costantini, 2016].

III. RESULTS

For as-grown YSZ samples, EPR spectra unambiguously show that HCs were generated upon UV-ray illumination (Fig. 1). These lines at g = 2.014, 2.011 (line 1) and g = 2.007 (line 2), are similar to those with $g > g_e = 2.0023$ for electron and ion-irradiated YSZ single crystals with the same magnetic-field orientation. It confirms previous conclusions that these defects were produced by electron-excitation processes induced by charged-particle irradiations. Note that no EPR signal was found in the virgin sample. Moreover, no defects were generated when UV-rays were filtered out from the white excitation spectrum of the lamp below a cut-off wavelength ~300 nm (i.e. $\hbar\omega \geq 4.1$ eV)). This means that such HCs were generated by above band-gap excitation processes. Similar short-time decays of the number of paramagnetic centres were found for both HC lines after UV-beam shut off (Fig. 2a).

For the Au-ion irradiated samples, a standard EPR spectrum was obtained with one line corresponding to HCs (line 2), and two lines for the F^+-type centres (g = 1.997, and g = 1.974) [Costantini, 2011]. The T centre line (g = 1.890) was not detected. The time-

dependence of the number of paramagnetic centres for all those lines is displayed for UV-light on and off for the 200-MeV Au ion irradiated sample at the fluence of 2.5×10^{13} cm^{-2} (Fig. 2b). It shows the appearance of line 1 (g = 2.011) upon UV-illumination for the maximum lamp power (P_{max}), followed by a clear exponential decay versus time down to a saturation level 20 minutes after that the UV-lamp was switched off. It has to be noted that line 1 was not present in the spectrum of the as-irradiated sample. It reached about the same intensity as line 2 under UV-lamp irradiation and remained at a constant level upon illumination. Instead, a non-reversible photo-annealing effect was seen for line 2 (g = 2.007) by a factor ~50% after growth to a saturation level at P_{max} (Fig. 2b). However, no effect was found on lines of F^+-type centres showing constant intensities for such broad-band photo-excitation (Fig. 2b).

In contrast, for the electron-irradiated sample, evidence for a photo-bleaching effect of F^+-type centres (g = 1.997 for B = 3506-3510 G, and g = 1.974 for B = 3547 G) was clearly found after selective excitation of the electron-irradiated sample with the LD system, irrespective of laser power (Fig. 3). No line of T centres was found like for the ion-irradiated sample. A saturation level was reached after decay for long-time laser irradiation (45 min.) (Fig. 4). No changes in the EPR spectra were observed after shutting off the laser beam, meaning that the photo-annealing effect was non-reversible. Moreover, this shows that it cannot be assigned to a thermal effect during the long-time illumination. Finally, no EPR signal arose in the virgin sample after laser irradiation at the maximum power of 105 mW for 25 minutes.

The evolution of the optical absorption band of F^+-type centres is shown for various annealing temperatures (Fig. 5). This broad band can be fit with a single Gaussian profile centred at ~550 nm, which is a characteristic absorption feature of these colour centres

[Costantini, 2004, 2010], in agreement with the EPR data showing no signal of T centres. Full thermal bleaching was achieved at 523 K.

IV. DATA ANALYSIS

Two clearly different decay behaviours were found for line 1 (g = 2.011) and line 2 (g = 2.007) of HCs in the 200-MeV Au-ion irradiated sample upon UV-lamp irradiation with two different asymptotic levels, starting from about the same number of paramagnetic centres (Fig. 2b). Line 1 corresponds to a transient defect that was unstable at RT, whereas line 2 underwent a partial photo-annealing effect. A striking difference was found for the virgin sample with similar irradiation conditions and about the same number of paramagnetic centres (Fig. 2a). These data can be fit by decay curves versus time to a non-zero asymptotic value, just like for T-centres after electron-beam irradiation and beam switch off [Costantini, 2014b]. The following function can be used for least-squares fitting of the number of paramagnetic centres (N) versus time (t):

$$N = N_0 + (N_\infty - N_0)\,[1 - e^{-(t-t_0)/\tau}] \qquad (1)$$

where N_0 and N_∞ are the starting value and asymptotic value, respectively, τ is the decay time constant, and t_0 is the time at onset of decay, either when the UV beam was shut off (for g = 2.011) or when photo-annealing occurs for P_{max} (for g = 2.007) (Figs. 2a-b). Similar time-decay behaviours were also found for F^+-type centres (g = 1.997, and g = 1.974) in the 1.4-MeV electron-irradiated sample upon laser excitation, with quite large τ values (~10 min) for the two EPR lines of the F^+-type centre (Table II), regardless of laser power (Fig. 4).

Similar decays are observed for the HC lines with shorter decay-time constants (τ ~1 min) and a ratio of the asymptotic value (N_∞) and starting value (N_0) ~ 0.3-0.5, except for line 1 showing a much stronger decay in the Au ion-irradiated sample with N_∞/N_0 = 0.03 (Table II). The rise time constants (τ') for growth of line 1 (Fig. 2b) and line 2 (Fig. 2a) are estimated to be ~2 min, by using a saturation function similar to Eq. (1). Since τ' and τ have similar values, we will assume that the growth and decay of these HCs involve the same processes under UV-beam illumination.

The normalized integrated intensity of the absorption band (Fig. 5) is plotted as a function of annealing temperature, in very good agreement with the normalized number of F^+-type centres deduced from EPR measurements (Fig. 6). Actually, these two sets of data for two different Au ion energies correspond to a similar color centre concentration (Table II). This confirms the assignment of the 2.4-eV absorption band to the F^+-type centres. These data are fit with a first-order kinetics giving an activation energy ΔE = 0.61 eV for the recovery process, that is quite consistent with previous determinations (~0.5 eV) [Costantini, 2006, 2014a].

V. DISCUSSION

Various kinds of behaviours of colour centres can be expected under photo-excitation, such as photo-conversion and photo-bleaching. For instance, in the case of F (i.e. F^0 or V_O^x) and F^+ ($V_O^\cdot$) centres produced by elastic collisions in MgO, a complex $F^+ \rightarrow F$ photo-conversion process takes place after UV-ray irradiation for photon energies ranging between 5 and 6 eV, below the band gap energy (E_g ~8 eV) [Kotomin, 1998]. In the present study, different behaviours are found for HCs and F^+-type centres upon illumination.

V. 1. Hole centres

For $\hbar\omega \geq E_g$, free electron-hole pairs are generated by above band-gap excitation, with subsequent electron or hole trapping on colour centres. Such kind of process may account for the partial UV-ray photo-annealing of the ion-induced OHC (line 1, for g = 2.007) with a short decay time constant (τ = 1 min.) (Fig. 2b). Moreover, the UV-induced HC (g = 2.011) was found to be unstable at RT in the ion-irradiated sample, but with a similar short decay time (τ = 2 min.) (Table II). We surmise that these defects are oxygen hole centres (OHCs), that may be different from the O^- centres with a strong g-factor anisotropy assigned to an orthorhombic symmetry site (with g_x = 2.019, g_y = 2.012, and g_z = 2.004). In the latter case, it was shown that O^- ions sit in a C_{2v} symmetry site with one native neighbour Y^{3+} ion (i.e. $[O_O^{\cdot} Y_{Zr}']^x$).

This hints to a mechanism of annihilation linked to ionization and free-electron trapping onto OHCs according to the following reaction: $O_O^{\cdot} + e' \rightarrow O_O^x$, where $O_O^{\cdot}$ stands for the OHC. Free-hole trapping onto oxygen ions (with the back reaction $O_O^x + h^{\cdot} \rightarrow O_O^{\cdot}$) leads to an equilibrium state corresponding to the asymptotic value of the decay curve. We assume that the growth process up to a saturation value involves the same reverse reactions, since τ and τ' time constants are similar (Table II).

Rate equations can be written for OHC growth and decay upon UV-ray excitation using free-electron or free-hole trapping on OHCs and oxygen ions (i.e. valence band states), respectively, as follows:

$$dN/dt = k_2 N_h - k_1 N \qquad (2)$$

$$dN_h/dt = R - k_2 N_h \qquad (3)$$

where R is the electron-hole pair production rate, N_h and N are the free hole and OHC numbers, respectively, k_1 is the rate constant for electron trapping on $O_O^{\cdot}$, and k_2 is the rate constant for hole trapping on O_O^{x}. The negligible second-order terms like $k_2 N_h N$ were discarded in Eq. (2).

An equation similar as Eq. (3) may be written for free-electron trapping on Zr^{4+} lattice ions with $N_e = N_h$ and rate constant k'_2, according to the reaction: $Zr_{Zr}^{x} + e' \rightarrow Zr_{Zr}'$. However, such a process may be neglected in the present study since no EPR signal of T centres was detected during illumination. This may arise from the long time constant for T-centre growth (τ' = 10 min) [Costantini, 2014a]. Charge-exchange processes with F^+-type centres can also be discarded since no changes of EPR lines of these colour centres were found upon UV-ray illumination (Figs. 2a-b).

Solution of Eq. (3) yields for the growth of free holes:

$$N_h = (R/k_2)\,(1 - e^{-t/\tau_2}) \qquad (4)$$

with a rise-time constant $\tau_2 = 1/k_2$, and a saturation for long time $N_{h,\infty} = R/k_2$, whereas solution of Eq. (2) gives for the growth of OHCs:

$$N = R/k_1 + \{N_0 - Rk_2/[\,k_1(k_2 - k_1)]\}\, e^{-t/\tau_1} + [R/(k_2 - k_1)]\; e^{-t/\tau_2} \qquad (5)$$

where $\tau_1 = 1/k_1$, $\tau_2 = 1/k_2$and $N_0 = N(t = 0)$.

For growth curves of both OHC lines from $N_0 = 0$, it gives an increasing function:

$$N = R/k_1 + [R/(k_2 - k_1)]\,[e^{-t/\tau_2} - (k_2/k_1)\,e^{-t/\tau_1}] \qquad (6)$$

with a saturation value $N_\infty = R/k_1$. If one process would dominate, Eq. (6) would reduce to a single exponential growth function.

The asymptotic values for free holes ($N_{h,\infty} = R/k_2$) and OHCs ($N_\infty = R/k_1$) at long illumination times should increase with R, i.e. the photon flux (φ) or lamp power (P), since $R = \varphi E/E_g \propto PE/E_g$, where E is the energy lost by photo-excitation for $\hbar\omega \geq E_g$.

When the UV beam is shut off, after saturation of growth up to $N_{h,\infty} = R/k_2$, for R = 0, a new set of equations must be used for OHCs and trapping of holes with similar approximations as above:

$$dN/dt = k_2 N_h - k_1 N \qquad (7)$$

$$dN_h/dt = k_1 N - k_2 N_h \qquad (8)$$

This implies that: $dN/dt + dN_h/dt = 0$ and thus $N + N_h = C$ (constant). Resolution of these two coupled differential equations yields:

$$N = N'_\infty + (N_s - N'_\infty)\,e^{-t/\tau} \qquad (9)$$

or

$$N = N_s + (N'_\infty - N_s)\,[1 - e^{-t/\tau}] \qquad (10)$$

similar to Eq. (1), where N_s is the OHC initial (saturation) number before beam shut-down, $N'_\infty = k_2\,C/(k_1 + k_2)$is the asymptotic value, and $\tau = 1/(k_1 + k_2)$ is the decay time constant.

To summarize, in this analysis, asymptotic values will depend on the free-electron trapping rate ($N_\infty = R/k_1$), whereas decay time constants (τ) will depend on respective effects of electron and hole trapping. This can explain the strong difference in saturation values found between the UV-induced centres and the ion-induced ones, even though the decay time constants may be similar (τ ~1-5 min) (Table II).

V. 2. F^+-type centres

Conversely, for F^+-type centres, much longer decay time constants (τ ~10-20 min.) (Table II) are found for the selective laser excitation at $\hbar\omega$ ~2.2 eV, inside the broad absorption band centred at ~2.4 eV (with FWHM ~1 eV) (Fig. 5). No significant difference was found between both EPR lines. Moreover, there is no clear evidence for a laser power effect or threshold from the present results.

We assume that photo-bleaching is likely related to the selective excitation of the trapped electron from the oxygen vacancy ($V_O^{\cdot}$). No such effect was found for the broad excitation spectrum with UV lamps generating electron-hole pairs (for $\hbar\omega \geq E_g$). In that case, the equilibrium value reached for long illumination time may result from the competition between the ionisation rate of the defect level in the band gap and the electron back-trapping rate onto oxygen vacancies.

For modelling the kinetics of isothermal annealing of F^+-type centres versus time for ion and electron-irradiated YSZ samples, we previously had to consider the charge exchanges between the three kinds of F centres: the neutral (F^0, or V_O^x), singly-ionized (F^+, or $V_O^{\cdot}$), and doubly-ionized (F^{2+}, or $V_O^{\cdot\cdot}$) oxygen vacancies, and T centres [Costantini 2014a]. Such analysis was needed to explain the maximum asymptotic value of paramagnetic F^+ centres (for long annealing times) as a function of annealing temperature. The low activation energy for

recovery (ΔE ~0.5 eV) was interpreted as the energy difference between F-centre levels in the band gap.

However, in the present case, no T centres were detected by EPR spectroscopy for both electron and ion-irradiated samples. As a result, we can consider charge trapping and emission on F^+ centres only, or charge exchanges between F centres to account for the equilibrium value at long illumination times. As mentioned in the introduction, this F^+-type centre is most likely an oxygen divacancy or F_2^+ centre ($[V_O^{\cdot} V_O^x]^{\cdot}$) for several reasons: i) g-factor anisotropy along <100>, ii) large spin-lattice relaxation time at low temperature, iii) large threshold displacement energy of oxygen atoms, iv) large defect volume [Costantini, 2011]. Accordingly, F^{2+} and F^0 centres are the associated divacancies with charge 2+ and null charge, respectively.

The photo-excitation for $\hbar\omega$ ~2.2 eV falls inside the broad absorption band of F^+-type defects centred at ~2.4 eV. It was found that the large FWHM (~1 eV) did not decrease when cooling down from RT to 10 K [Costantini, 2004]. This behaviour was assigned to the major effect of the intrinsic disorder (native oxygen vacancies, $V_O^{\cdot\cdot}$) on the band width, with negligible effect of phonons. A similar behaviour was found for the T-centre absorption band (centred at ~3.2 eV) [Azzoni, 1995], and band-gap energy [Camagni, 1992]. Instead, the band-gap energy of YSZ strongly depends on the yttria content, i.e. on the oxygen vacancy concentration [Camagni, 1992].

Actually, the optical gap (E_g ~4.2 eV for 9.5 mol% Y_2O_3) corresponds to an "apparent" band gap due to energy levels linked to yttrium impurities, lying below the conduction band edge. The "true" band gap for pure ZrO_2 is ~6 eV, as determined by EELS spectroscopy [French, 1994]. Optical absorption of F^+-type defects corresponds to transitions from a deep gap state to these levels that are distributed in a continuum due to static disorder.

As a result, since $\hbar\omega \sim E_g/2$, the electron trapped in the F^+ centre energy level must be photo-excited from a mid-gap state to an excited state lying in the broad distribution of energy levels near the conduction band edge. Moreover, various calculations give an energy difference ($\Delta\varepsilon$) between levels of $F^{0/+}$ and $F^{+/2+}$-type centres ranging between 0.2 eV [Foster, 2001; Robertson, 2005] and ~0.9 eV [Stapper, 1999; Muñoz-Ramo, 2008], according to different approximations. Such small values are similar to the energy differences between levels of F-centres that were inferred from thermal annealing curves [Costantini, 2014a]. Since $\hbar\omega > \Delta\varepsilon$, the excited electron can decay from excited states either to the $F^{0/+}$ level or the $F^{+/2+}$-level (Fig. 7).

Therefore, we will assume that the origin of photo-bleaching of paramagnetic F^+-type centres can be attributed to ionization of the $F^{0/+}$ level and subsequent free electron trapping on F^+ and F^{2+}-type centres with numbers N_1 and N_2, respectively, under selective laser excitation. The rate equations for the free electron number (N_e) and the defect populations can be written as:

$$dN_e/dt = G N_1 - k N_1 - k' N_2 \quad (11)$$

$$dN_1/dt = - G N_1 - k N_1 + k' N_2 \quad (12)$$

$$dN_2/dt = - k' N_2 + G N_1 \quad (13)$$

$$dN_0/dt = k N_1 \quad (14)$$

where N_0 stands for the neutral F^0 centre concentration, and G, k and k' are the rate constants for ionization and electron captures on the two levels, respectively. Two-body terms were also neglected as for the HCs. These coupled differential equations imply that $N_1 + N_2 + N_0 + N_e$ = constant, and yield a decay for the F^+ type centres with an equilibrium non-zero asymptotic value. Hence, the resulting time-decay behaviour will depend on the relative effects of ionization and electron trapping. However, this would give a dependence of the decay time constant on G, which is not in agreement with experimental data (Table II). Therefore, we assume that the decay should involve another defect, probably HCs trapping the electrons upon photo-excitation. This may also explain that both zero and non-zero asymptotic values can be reached upon photo-bleaching for the different samples.

VI. CONCLUSIONS

Stable hole centres (HCs) were produced in as-grown YSZ single crystals by UV-ray irradiation at RT, as shown by two EPR lines at g = 2.007 and g = 2.011. These two lines decay to a saturation value after UV beam shut off. The first line, also produced after 200 MeV Au-ion irradiation, showed a partial photo-bleaching by ~50% under UV light in the same conditions. However, the second line was not produced by ion irradiation. The latter line was produced upon UV-ray irradiation, and quickly decayed to a low saturation value after UV-beam shut off. No effect of UV light was found on the two EPR lines (g = 1.974, 1.997) assigned to F^+-type centres. Instead, laser irradiation at 553 nm wavelength of an electron-irradiated sample induced full or almost full photo-bleaching effect of F^+-type centres by photo-excitation inside the characteristic absorption band. No evidence of laser power was found on decay time constants and asymptotic values for both EPR lines. Complete thermal bleaching of F^+-type centres was achieved at ~500 K. Kinetic rate models

of defect evolutions are proposed to account for photo-induced recovery effects, on the basis of charge exchanges between point defects.

ACKNOWLEDGMENTS: We thank the French EMIR network for supporting this research program. The authors are also indebted to Kurt Schwartz (Helmholtz Centre for Heavy Ion Research, Darmstadt, Germany) for the Au ion irradiation at GSI-UNILAC, and to Bruno Boizot (École Polytechnique, Palaiseau, France) for his help during the electron irradiation.

Table I: Irradiation features of 500 μm thick YSZ samples: inelastic stopping power $(-dE/dx)_{inel}$, total absorbed dose (D), and total number of displaced oxygen atoms (N_d) in the irradiated volume (V) [Costantini, 2011a].

Particle	V (cm^3)	Energy (MeV)	$(-dE/dx)_{inel}$ (MeV μm^{-1})	Range (μm)	Fluence (cm^{-2})	D (eV cm^{-3})	N_d	N_d/V (cm^{-3})
e^-	0.008	1.4	$7.9x10^{-4}$	$1.7x10^3$	$2.1x10^{18}$	$1.6x10^{19}$	$\sim 1x10^{17}$	$\sim 1.25x10^{19}$
^{197}Au	0.05	200	32.7	10	$2.5x10^{13}$	$8x10^{18}$	$\sim 1x10^{18}$	$\sim 2x10^{19}$
^{197}Au	0.05	200	32.7	10	$1x10^{12}$	$3x10^{17}$	$\sim 4x10^{16}$	$\sim 8x10^{17}$
^{197}Au	0.19	2240	38.2	59	$1x10^{12}$	$4x10^{17}$	$\sim 7x10^{16}$	$\sim 4x10^{17}$

Table II: Decay (τ) and rise (τ') time constants, and ratio of the saturation (N_∞) and starting number of paramagnetic centres (N_0) for: oxygen hole centers OHC (g = 2.007, 2.011) in the virgin YSZ (v) and Au-ion irradiated (Au) YSZ single crystal sample, F^+-type centres (g = 1.974, 1.997) in the 1.4-MeV electron-irradiated sample (e^-) for various laser powers (P).

YSZ	^{197}Au	v	^{197}Au	v	e^-	e^-	e^-		e^-
Sample name	AU14		AU14		YSZ-6	YSZ-5	YSZ-6		YSZ-5
Colour centre	OHC	OHC	OHC	OHC	F^+	F^+	F^+		F^+
Excitation	UV	UV	UV	UV	laser	laser	laser		laser
g	2.011	2.011	2.007	2.007	1.997	1.997	1.974		1.974
P (mW)	/	/	/	/	52	105	52		105
τ (min.)	2	5	1	1	12	12	8		11
N_∞ / N_0	0.03	0.37	0.40	0.45	0.24	0	0		0
τ' (min.)		1.7	1.7						

REFERENCES

[Azzoni, 1989] C. B. Azzoni, and A. Paleari, Phys. Rev. B **40**, 6518 (1989).

[Azzoni, 1991] C. B. Azzoni, and A. Paleari, Phys. Rev. B **44**, 6858 (1991).

[Azzoni, 1995] C. B. Azzoni, and A. Paleari, Phys. Rev. B **51**, 15942 (1995).

[Azzoni, 1996] C. B. Azzoni, A. Paleari, G. Samoggia, and F. Scardina, Phys. Rev B **51**, 15942 (1996).

[Biersack, 1980] J. P. Biersack, and L. G. Haggmark, Nucl. Instr. and Meth **174** (1980) 257.

www.srim.org

[Camagni, 1992] P. Camagni, P. Galinetto, G. Samoggia, and N. Zema, Solid St. Commun. **83** (1992) 943.

[Chassé, 2015] M. Chassé, G. Lelong, P. van Nijnatten, I. Schoofs, J. de Wolf, L. Galoisy, and G. Calas, Appl. Spectrosc. **69**, 457 (2015).

[Costantini, 2004] J. M. Costantini, F. Beuneu, D. Gourier, C. Trautmann, G. Calas, and M. Toulemonde, J. Phys.: Condens. Matter **16**, 3957 (2004).

[Costantini, 2006] J. M. Costantini, and F. Beuneu, J. Phys.: Condens. Matter **18**, 3671 (2006).

[Costantini, 2010] J. M. Costantini, F. Beuneu, K. Schwartz, C. Trautmann, J. Phys.: Condens. Matter **22**, 315402 (2010).

[Costantini, 2011] J. M. Costantini, and F. Beuneu, J. Phys.: Condens. Matter **23**, 115902 (2011).

[Costantini, 2013] J. M. Costantini, and F. Beuneu, Nucl. Instr. and Meth. B **314**, 130 (2013).

[Costantini, 2014a] J. M. Costantini, F. Beuneu, and W. J. Weber, Philos. Mag., **94** (2014) 2281.

[Costantini, 2014b] J. M. Costantini, M. Fasoli, F. Beuneu, and B. Boizot, Philos. Mag., **94** (2014) 4053.

[Costantini, 2016] J. M. Costantini, G. Lelong, M. Guillaumet, W.J. Weber, S. Takaki, and K. Yasuda, J. Phys.: Condens. Matter, **28** (2016) 325901.

[Foster, 2001] A. S. Foster, V. B. Sulimov, F. Lopez Gejo, A. L. Shluger, and R. M. Nieminen, Phys. Rev B **64**, 224108 (2001).

[French, 1994] R. H. French, S. J. Glass, F. S. Ohuchi, Y. N. Xu, and W. Y. Ching, Phys. Rev. B **49** (1994) 5133.

[ICRU, 1984] "*Stopping Powers for Electrons and Positrons*", International Commission on Radiation Units and Measurements ICRU Report 37 (1984). (http://physics.nist.gov/PhysRefData/contents-radi.html).

[Kotomin, 1998] E. A. Kotomin, and A. I. Popov, Nucl .Instr. and Meth. B. 141 (1998) 1.

[Merino, 1989] R. I. Merino, V. M. Orera, E. E. Lomonova, and S. Kh. Batygov, Phys. Rev B **40**, 8555 (1989).

[Muñoz-Ramo, 2008] D. Muñoz Ramo, P. V. Sushko, J. L. Gavartin, and A. L. Shluger, Phys. Rev B **78**, 235432 (2008).

[Orera, 1990] V. M. Orera, R. I. Merino, Y. Chen, R. Cases, and P. J. Alonso, Phys. Rev. B **42**, 9782 (1990).

[Robertson, 2005] J. Robertson, Ka Xiong, and B. Falabretti, IEEE Trans. on Device and Materials Reliability, **5** (2005) 84.

[Stapper, 1999**]** G. Stapper, M. Bernasconi, N. Nicoloso, and M. Parrinello, Phys. Rev. B **59** (1999) 797.

[Zacate, 2000] M. O. Zacate, L. Minervini, D. J. Bradfield, R. W. Grimes, and K. E Sickafus, Solid State Ionics **128**, 243 (2000).

Fig. 1: EPR spectrum (with B // <100>) of an as-grown (100) YSZ single crystal upon UV-light irradiation at RT.

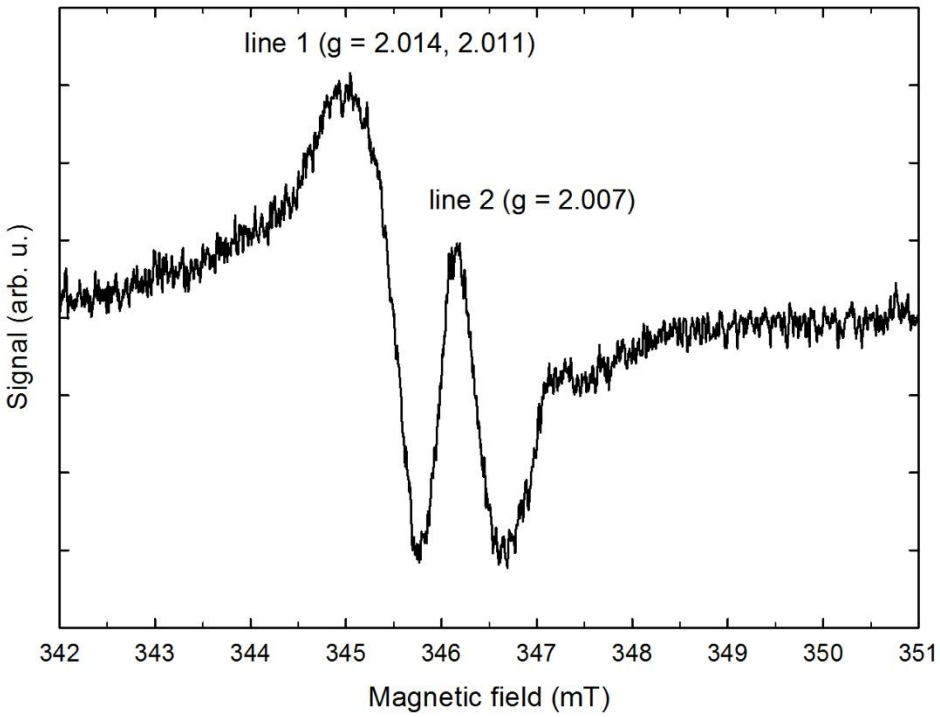

Fig. 2a: Time-dependence of EPR lines of hole centres (g = 2.007, 2.011) for a virgin (100) YSZ single crystal upon UV illumination at RT. Dashed lines are fitted growth and decay curves.

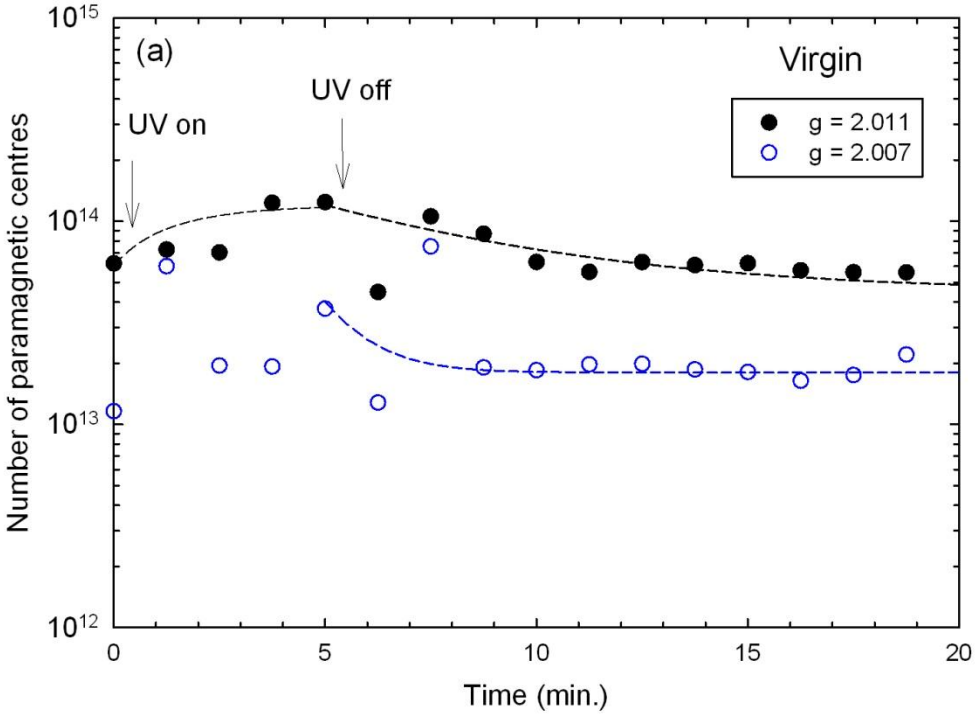

Fig. 2b: Time-dependence of EPR lines of hole centres (g = 2.007, 2.011) and F^+-type centres (g = 1.974, 1.997), for the 200-MeV Au ion irradiated (100) YSZ single crystal upon UV illumination at RT. Dashed lines are fitted exponential growth and decay curves.

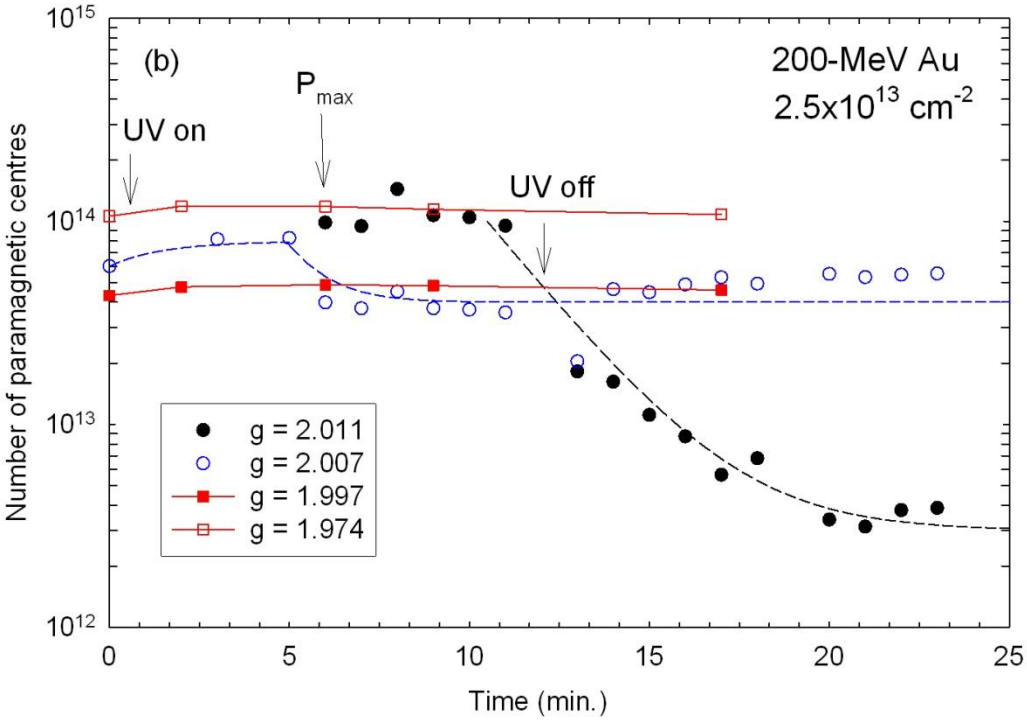

Fig.3: EPR spectra (with B // <100>) of the 1.4-MeV electron-irradiated (100) YSZ single crystal before and after laser illumination at RT.

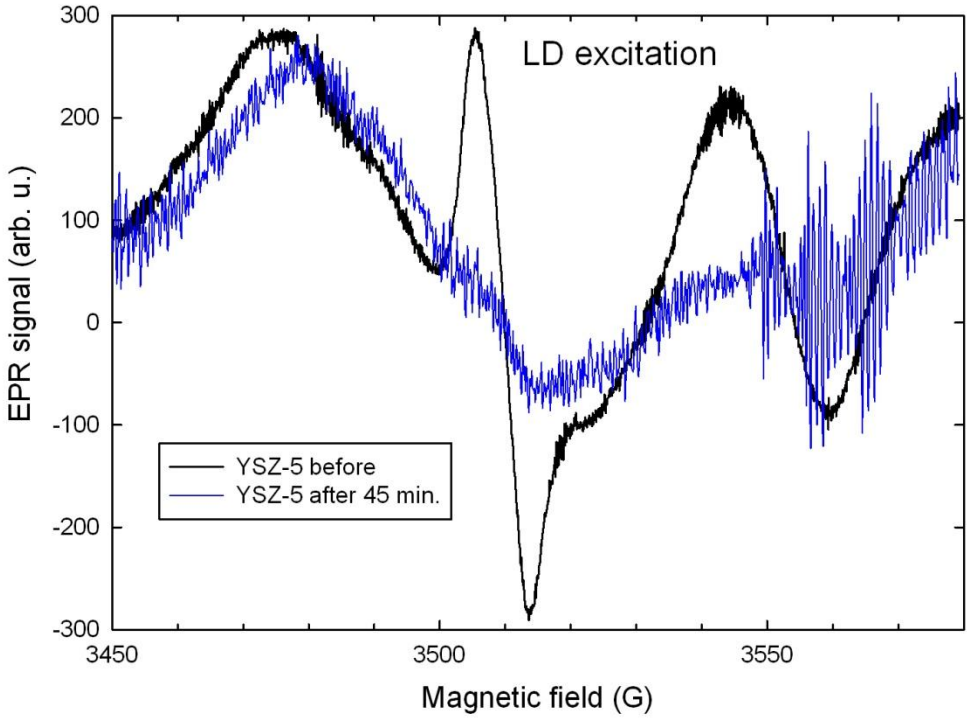

Fig. 4: Time-dependence of EPR lines of F^+-type centres (g = 1.974, g = 1.997), for the 1.4-MeV electron-irradiated (100) YSZ single crystal upon laser illumination at RT for various power values. Solid lines are fitted exponential decay curves.

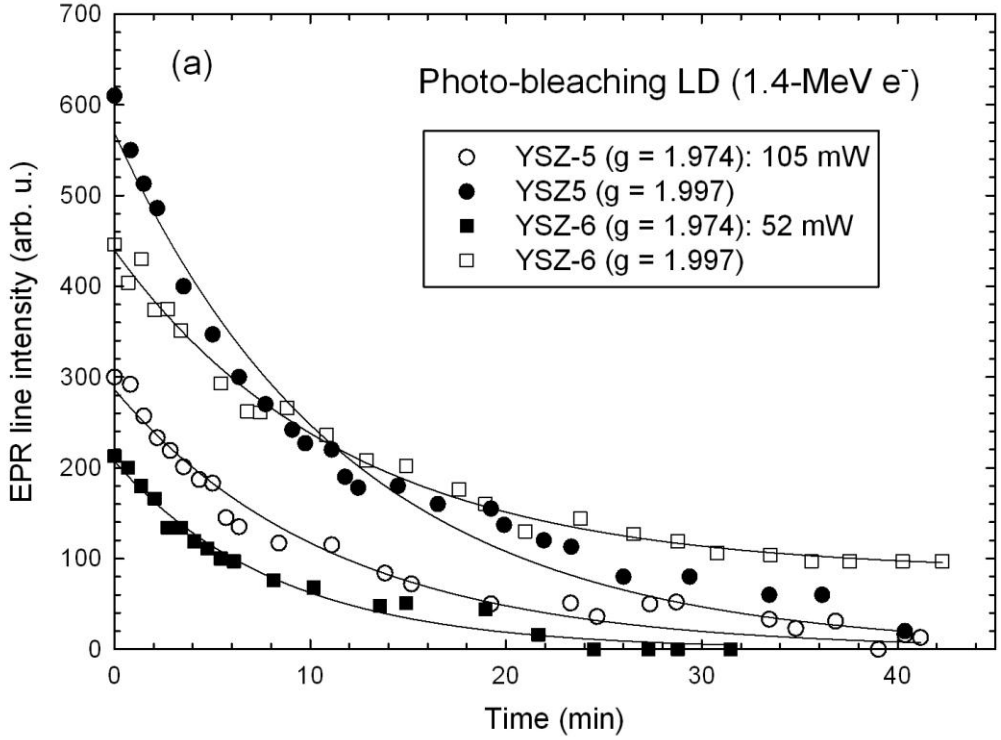

Fig. 5: UV-visible absorption spectrum of the 2.24-GeV Au ion irradiated YSZ sample (fluence = 10^{12} cm^{-2}) as-irradiated at RT and for subsequent annealing for various temperatures. Solid black lines are Gaussian fits.

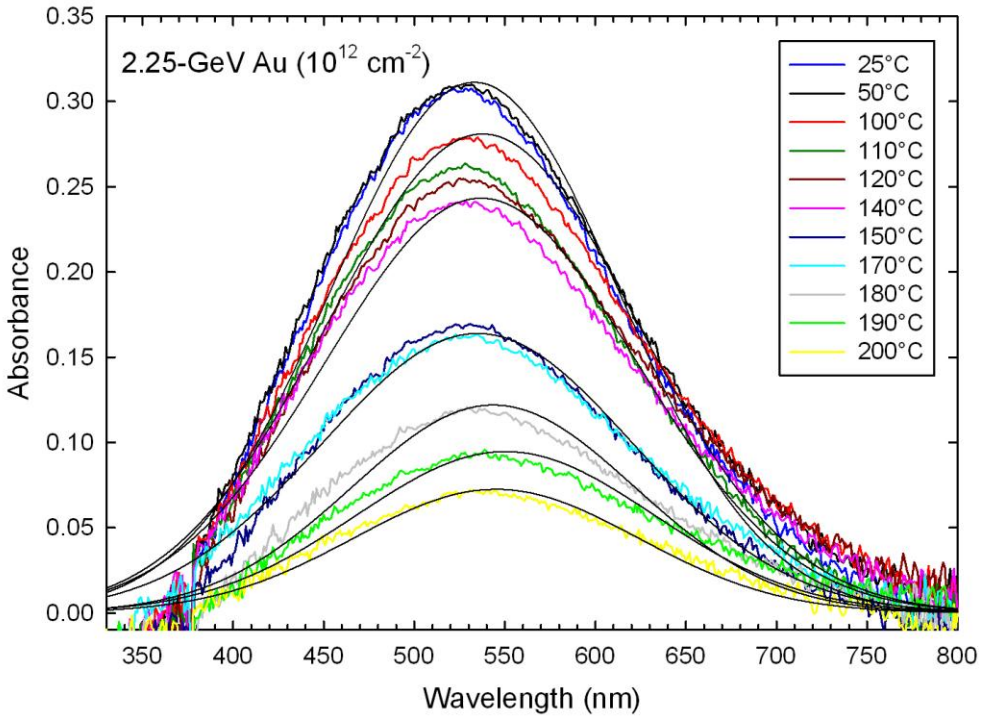

Fig. 6: Normalized integrated intensity (full circles) of the 2.4 eV absorption band for the 2.24-GeV Au ion irradiated YSZ sample (fluence = 10^{12} cm^{-2}), and normalized number of F^+-type centres (open triangles) deduced from EPR data for the 200-MeV Au ion irradiated YSZ sample (fluence = 10^{12} cm^{-2}) versus annealing temperature. The solid line is a least-squares fit of the optical absorption data.

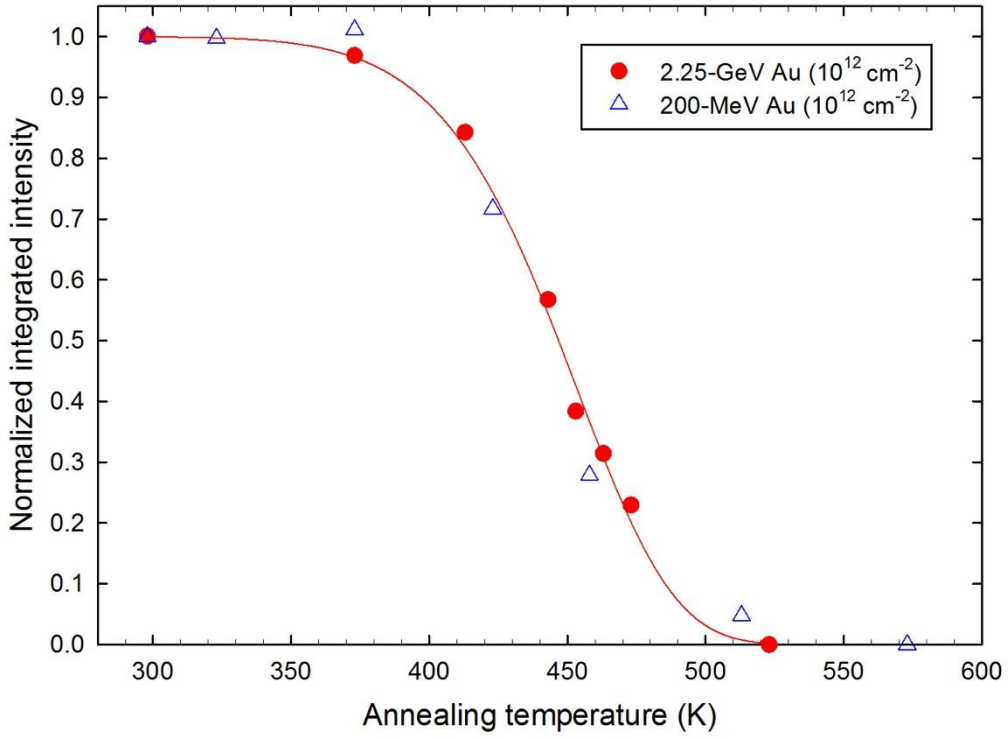

Fig. 7: Schematics of F^+-type centre energy levels (without relaxation) in the YSZ band gap (E_g ~4.2 eV).